MJO Simulated by a CGCM: Sensitivity of Mean State Climate and Basin-Scale Air-Sea Coupling

Shu-Ping Weng[1], Jin-Yi Yu[2]
[1]Department of Geography, National Taiwan Normal University
[2]Department of Earth System Science, University of California, Irvine

Abstract

This study examines the impacts of Indian and Pacific Ocean coupling on the zonal propagation of Madden-Julian oscillation (MJO) during the cold seasons (NDJFMA). A series of basin-coupling experiments are performed with the UCLA coupled atmosphere-ocean general circulation model (CGCM), in which the atmosphere-ocean coupling is limited to the Indian Ocean (IO Run), the Pacific Ocean (PO Run), or the Indo-Pacific Ocean (IP Run). Results of EEOF analysis indicate that MJO-related rainfall and circulation anomalies in all experiments are sensitive to the biases of tropical mean westerlies and cold SSTs over the Maritime Continent and West Pacific (WPAC). It is further shown that having a realistic background flow is only a necessary condition to sustain a realistic MJO. Although the mean westerlies well extend from the central Indian Ocean to the SPCZ in the PO Run, simulated MJO-related convection tends to be initiated locally in the equatorial WPAC when the Indian Ocean's coupling is absent. Without the Pacific Ocean's coupling, on the other hand, the simulated convection in the IO Run can not penetrate eastward beyond the Maritime Continent. In stead, the associated low-level circulation tends to be bifurcated poleward as approaching the western Maritime Continent mainly due to the deficiency of diminishing background westerlies off the coasts of Sumatra. Only allowing the coupling presenting in both Indian and Pacific Oceans can the propagating features simulated by the IP Run somewhat resemble the observed MJO.

Key word: Coupled GCM, Madden-Julian Oscillation, Extend EOF

1. Introduction

A mounting body of observational studies showing the coherent fluctuations between the surface flux and SST associated with the MJO (Madden and Julian 1994) has prompted the explanation that MJO is a coupled phenomenon rooted in the interactions between the atmosphere and warm oceans (Woolnough et al. 2000). This emerging consensus is heuristically bolstered by the observed variability of its propagation direction associated with the seasonally varying basic circulation and SST distribution. When the distribution of wintertime warm pool SSTs is more or less symmetric to the equator, MJO propagation is primarily eastward. For a strong event, it redevelops over the western Pacific warm pool (WPWP) and often intersects the SPCZ where the warm SSTs reside (Wang and Rui 1990).

To obtain a realistic MJO simulation therefore, the AGCM should be coupled to some form of the oceanic model as suggested by the theoretical works (Wang and Xie 1998) and coupled model experiments (Flatau et al. 1997; Waliser et al. 1999). These studies concluded that the coupling not only provides an energy source to destabilize the atmospheric low-frequency perturbations but also serves as a scale selection mechanism favouring the large scale eastward propagating component. Inness et al (2003) showed that the third Hadley Centre fully Coupled GCM can reproduce the observed features of the MJO in many respects. However, it is not the case in the forced simulations of atmosphere-only version of the same GCM (HadAM3) driven by the observed SSTs. The incapability of modeling the observed MJO by most AMIP-type AGCM runs has been extensively discussed (Slingo et al. 1996; Waliser et al. 2003).

Nevertheless, contrasting model results concerning the relative importance between air-sea coupling and atmospheric internal dynamics to a realistic MJO simulation appear in the literature. In the case of GFDL AGCM interacting with a 1-D ocean mixed layer model, for example, Hendon (2000) concluded that coupling has minimal impacts on the MJO simulation since the anomalies of surface latent heat flux in response to the intraseasonal surface wind stress variations are relatively weak. With a modified convection scheme, Maloney (2002) also showed that NCAR AGCM (CCM3.6) is able to reproduce the eastward propagating MJO-related convection in the absence of an interactive ocean. Constrained by the prescribed SSTs, AGCMs may have a realistic basic state but very likely brings in biases while coupling an interactive ocean due to the increased number of degree of freedom and in turn affect the simulated MJO. Therefore, above results imply that a reasonable MJO simulation is preconditioned by a realistic CGCM climate as suggested by some recent studies (Kemball-Cook et al. 2002; Inness et al. 2003) and reemphasized in current study.

It is of interest in current study to further examine the following two hypotheses raised from previous works regarding the role of basin-coupling. 1) MJO is bred from the air-sea coupling in the Indian Ocean. 2) Effect of Pacific Ocean coupling is crucial for sustaining its eastward propagating feature. Our goals will be achieved by contrasting the results between different basin

coupled experiments described below.

2. CGCM experiments and methodology

The CGCM (detailed in Yu and Mechoso 2001) used in current study consists of the UCLA AGCM and GFDL Modular Ocean Model. The UCLA AGCM is global coverage with a horizontal resolution of 4° (lat.) by 5° (long.) and 15 levels in the vertical with the top at 1 mb. The GFDL MOM has a long. resolution of 1° and a lat. resolution varying gradually from 1/3° between 10°S and 10°N to about 3° at both 30°S and 50°N. It has 27 layers in the vertical with 10-m resolution in the upper 100 m. No flux adjustment is applied to the information exchange between atmospheric and oceanic component. Three experiments are performed to examine the effects of individual ocean basin coupling on the MJO characteristics: the Pacific Ocean (PO) Run, the Indian Ocean (IO) Run, and the Indo-Pacific (IP) Run. In the PO Run, the CGCM includes only the Pacific Ocean (30°S–50°N, 130°E–70°W) in its ocean model domain. The IO Run includes only the Indian Ocean (30°S–50°N, 30°–130°E), whereas the IP Run includes both Indian and Pacific Oceans (30°S–50°N, 30°E–70°W) in the ocean model domain. Outside the ocean model domains, we exclude any effect of air-sea interactions by specifying climatological monthly mean SSTs. Inside the ocean model domains, SSTs poleward of 20°S and 30°N are relaxed toward their climatological values. Above IP, PO, and IO Runs are integrated for 59, 52, and 58 yr, respectively. Only the daily archive of the last 30 yr is used in current study.

The procedure used to extract out the MJO signal from the daily data is as follows. The normal annual cycle is first determined by the sum of the first three harmonics of mean daily time series. Subtracting this normal annual cycle from raw daily data yields the daily anomaly. The interannual variation estimated by 3-month weighted monthly-mean anomaly is then removed from the daily anomaly before computing the 5-day mean pentad anomaly. This results in the variations with the intraseasonal timescale ranging from 10 days to 3 months. To make comparisons, the CMAP precipitation dataset is also processed in an analogous way but taking the factor of its pentad-resolution into account. The interrelationship between MJO and ENSO is an important issue to the seasonal prediction but is still yet to be fully understood. Aiming at investigating how the propagating nature of MJO is influenced by the basin scale coupling, we thus intentionally removed any possible effect of interannual variability from data in current study.

The canonical structure of MJO-related large-scale variations is identified by the extended EOF analysis (EEOFA). To select the composite cases, positive and negative 5 pentad lags anomalies of the easterly vertical shear (EVS; i.e., $u'_s \equiv u'_{200} - u'_{850}$) in the tropical eastern hemisphere (20°S-to-20°N, 30°E-to-180°E) during the thirty NDJFMA seasons are subjected to the EEOFA to identify the dominant 'mode' in the intraseasonal timescale. The first pair of eigenvectors mainly describes the MJO-related activity. The composite MJO life cycle is then constructed by averaging the first 40 (20/20) strong events having the largest peak (positive/negative) amplitudes in the corresponding PC time series. Above composite procedure is repeatedly applied to individual CGCM experiments as well as the observations.

3. CGCM climates

The left panels of Fig. 1 show the observed 200-mb (Fig. 1a) and 850-mb (Fig. 1b) mean wind fields in ERA40, and NOAA OISST_v2 climatology (Fig. 1c). Shown in the right panels of Fig. 1 are the corresponding IP Run climatology of the equivalent fields (Figs. 1d-1f). Shaded areas in the 200-mb (Figs. 1a and 1d) and 850-mb (Figs. 1b and 1e) winds are the mean EVS and rainfall estimates, respectively. In addition, zeros of EVS are outlined as thick solid lines and tropical low-level westerlies are emphasized as white vectors. With the same configurations as those in Fig. 1, the left and right panels of Fig. 2 show the climatology generated by PO and IO Runs, respectively.

Although the gross features of basic state produced by this particular CGCM are quite realistic, some large errors in the mean 3-D circulation and SST fields are evident. Compared to observations, SSTs in the IP Run are too warm in the equatorial north Pacific and eastern Pacific cold tongue regions; but too cold over the Arabian Sea, Bay of Bengal (BoB), and South China Sea (SCS). Warmer WPWP is also erroneously displaced eastward accompanied by a too-zonal SST pattern that extends too far into the southeastern Pacific. Perhaps the largest error that affects the simulated eastward propagating MJO is the cold bias of SST in the tropical Indian Ocean and especially the Maritime Continent regions (larger than -2°C). These erroneous SST features found in the IP Run are also common to the PO Run in the Pacific basin and IO Run in the Indian Ocean basin. Additionally, the PO (IO) Run in general has even warmer (colder) SST maxima in the Pacific (Indian) Ocean basin while lacking the air-sea coupling of the Indian (Pacific) Ocean as compared to the IP Run.

Errors of the mean tropical rainfall pattern in the IP Run are closely related to the SST errors, with a deficient in the western Maritime Continent over colder SSTs and excessive precipitation in the eastern extension of SPCZ and equatorial Pacific ITCZ regions in response to the underlying warmer SST. Above features are also evident in the former region of IO Run and in the latter regions of PO Run, demonstrating the in-phase relationship between the tropical mixed-layer SST and rainfall variability. Conversely, substantial errors of excessive precipitation in the tropical Indian Ocean produced by IP and IO Runs could be related to the systematic error in the Maritime Continent through the atmospheric Walker circulation and likely contribute to the aforementioned cold SST bias therein. Compared to the IP Run, however, the PO Run underestimates the oceanic precipitation in the tropical Indian Ocean whereas the IO Run overestimates the precipitation in the

WPWP regions while lacking of an interactive ocean, implying the equatorial ocean dynamical process acting differently between the surface westerlies in the Indian Ocean and easterlies in the central Pacific. In these regions, maximum convection centers also tend to locate near some large islands, indicating the dominant contribution of diurnal topographic forcing.

While the majority of coupled models has an easterly bias over the WPAC, a crucial factor that acts to block the eastward propagating MJO (Inness et al. 2003), results of mean 850-mb winds show the extent of westerlies in the WPAC to be well captured in our coupled experiments (c.f., middle panels of Figs. 1 and 2). This is directly linked to the erroneously eastward displacement of warmer SSTs in the SPCZ regions. On the other hand, diminishing westerlies on and just south of the equator in the eastern edge of Indian Ocean is an outstanding feature of both IP and IO Runs, with the westerlies being weakest and changing into easterlies in the IO Run. As a result, a peanut-shaped EVS straddling the equator is evident in the 200-mb circulation pattern of IP Run and is so weak as to be splitted in the IO Run. Besides the model deficiencies in representing the local air-sea-land interactions, systematic easterly bias near the Sumatra and cold SST in the SCS-Maritime Continent are also related to the errors at higher latitudes revealed by the stronger northeasterly winter monsoon that intrudes southward into the equatorial SCS and by the equatorward shift of East Asian jets.

4. Simulated MJOs

Figure 3, 4, 5, and 6 show the evolution of 850-mb wind and rainfall (color-shaded) anomalies depicted by the observation (ERA-40 plus CMAP), IP, PO, and IO Runs, respectively. To save our space, however, only one half of its life cycle between -25-day (i.e., phase 1) and 0-day (i.e., phase 6) are presented. Readers can refer to the same figures but with opposite sign for the next half cycle. Only color-shaded areas and the black vectors significant at 95% (90%) level are shown for the observed (simulated) MJO. For completeness, anomalous winds that are statistically insignificant are also shown as gray vectors.

As described by Rui and Wang (1990) and many others, observed life cycle of MJO-related rainfall anomalies in CMAP data showing a four-stage development process: 1) initiation over equatorial Africa (and/or western Indian Ocean), 2) rapid intensification when passing through the Indian Ocean, 3) mature evolution characterized by a weakening in the Maritime Continent and redevelopment over the WPAC, and 4) dissipation when approaching the date line in moderate events or emanation from the equator toward North America and southeastern Pacific (and SPCZ) in strong events, is faithfully reproduced in Fig. 3. Also evident in the phasing of equatorial low-level circulation to enhanced rainfall activity includes: 1) concentrated westerly anomalies and a pair of off-equator cyclonic circulations coupling with rainfall anomalies in between propagate eastward before reaching the East Pacific, 2) convergent center tends to lead the maximum rainfall during the developing and mature phases, and 3) the maximum westerly anomalies tend to lag rainfall anomalies during the developing phase, but almost overlap during the mature phase and lead the rainfall anomalies in dissipation phase.

Additional features are also noted when the rainfall anomalies approach the Sumatra and just pass through the Maritime Continent. In these phases, a dipole of rainfall anomalies with an opposite sign appears in the BoB and Philippine Sea. The former (latter) is initiated (detached) from the northward extension (northwestward branch) of equatorial eastward propagating rainfall anomalies (phase 4-to-6). Although dissipate rapidly, they are unique since there are no counterparts in the wintertime of southern hemisphere and thereby signify stronger tropical–extratropical interactions mainly due to the stronger Asian winter monsoon.

Although the area of large intensity is much smaller, composite MJO life cycle in some aspects of low-level wind and rainfall anomalies simulated by the IP Run (Fig. 4) does resemble the observations. Rainfall anomalies initiated in the equatorial Africa and propagating eastward from the Indian Ocean to Maritime Continent are reproduced (phase 1-to-3). Meanwhile, the associated intensified equatorial westerly (easterly) anomalies also tend to lag the enhanced (suppressed) rainfall anomalies during this developing phase. Moreover, the enhanced rainfall and the lagged westerly anomalies capable of passing around the Maritime Continent from the south and later heading toward the WPWP-SPCZ regions are particularly encouraging (phase 4-to-6). Lacking of basic-state low-level westerly winds over the WPAC and cold SST in the central Pacific has been suggested by Inness et al. (2003) as the main reasons why a CGCM is unable to reproduce a MJO-related convection propagating from the Indian Ocean into the WPAC. With the basic-state westerly winds well extending into the SPCZ (Fig. 1e) and warm SST in central Pacific south of equator (Fig. 1f), features of model MJO around and south of the equator indeed support such a viewpoint.

However, larger errors are found in the northern hemisphere (NH). Rainfall pattern near the equator is dominated by a mixture of eastward propagating convection anomalies initiated in the southern portion of SCS (phase 5) and westward propagating anomalies that flare up one pentad later over the East Pacific ITCZ (phase 6). Both meet together near the date line (phase 4) and thereby form a spuriously standing oscillation. In addition, the observed dipole of oceanic rainfall anomalies appearing in the BoB and Philippine Sea is erroneously shifted westward to the Arabian and Indo-China peninsulas, respectively. During this process, a synoptic-scale wave train pattern emerging from Asia, crossing the North Pacific sector towards North America is associated with somewhat loosen-up equatorial large-scale wind anomalies. Note that the initial flaring of convection in the East Pacific ITCZ slightly lags the one in the SCS, suggesting that the former and its rapid

westward extension is likely excited and maintained by the extratropical forcing of Rossby wave energy emerging from the exit of Asian-Pacific jetstream. The rectification of extratropical transient disturbances onto the tropical MJO has been emphasized by previous studies (e.g., Hsu et al. 1990; Matthews and Kiladis 1999). An important conclusion is that the CGCM used in this study apparently exaggerates such a scenario due to its "colder" basic state thereby affects the eastward propagating component in the deep tropics of NH.

Dramatic changes occur when an interactive Indian Ocean is absent in the PO Run (Fig. 5). *Firstly*, there exists barely evidence of eastward propagating rainfall anomalies followed by the wind anomalies in the equatorial Indian Ocean regardless of the existence of mean westerly winds that well extend from Indian Ocean into the WPAC (Fig. 2b). In stead, suppressed rainfall anomalies stalling over the western Indian Ocean and the stationary even somewhat retrograded westerly anomalies over the equatorial eastern Indian Ocean and Maritime Continent are interpreted as parts of upstream atmospheric response to the intraseasonal SSTA forcing over the WPWP-SPCZ regions through changing the east-west Walker circulation. It thus suggests that the appearance of mean westerly winds is only a necessary condition for sustaining a realistic MJO event. *Secondly*, having the air-sea coupling only in the Pacific Ocean, the PO Run (compared to IP Run) on one hand reproduces smaller ISV over the WPAC due to the lack of MJO propagating in from the Indian Ocean, but on the other hand shows its excessive footprints both on the extended propagation from the WPWP towards SPCZ east of date line and on the enhanced convectively coupled waves (Matthews and Kiladis 1999) propagating from the central Pacific along the equatorial wave guide towards North America, which are consistent with the warmer ($\geqq$1°C) basic state SSTs therein (see Fig. 2c).

Finally, it is of interest to note how a Rossby-wave-like pattern is formed across the entire Indo-Pacific sector in the tropical-to-subtropical latitudes of NH (phase 5). Lacking of air-sea coupling to the west of 130°E, an anomalous cyclonic circulation anchored over the Asian landmass is accompanied by an anomalous anticyclonic circulation initially emerged from equatorial East Africa. This anticyclonic anomaly moving slowly northwestward represents the off-equator Gill-type solution in response to negative tropical forcing (i.e., suppressed rainfall anomalies in its southeast corner). With the coupling to the east of 130°E, however, a northwestward migrating cyclonic circulation anomaly is emitted from the equatorial central Pacific and later wedges itself into the wave train pattern. Note also the rapid dissipation of equatorial anomalies after phase 5. The result in PO Run is thus characterized by a serial synoptic-scale wave activity in NH and does not complete the cycle, implying the MJO is rooted in the air-sea coupling over Indian Ocean.

Although having a faster pace and being more constrained within the oceanic portion, the general pattern of rainfall and low-level circulation anomalies in the IO Run (Fig. 6) resembles those in the IP Run (Fig. 4) until the rainfall anomalies are approaching the Sumatra in phase 4. It is right in this location that the basic-state westerly winds diminish and change into easterlies (Fig. 2e), supporting the paradigm that dismissal of mean westerlies near Maritime Continent from a CGCM climatology signifies the barrier for MJO in its journey towards WPAC. Concurrent with the intensified rainfall anomalies in the eastern Maritime Continent in phase 4 are the enhanced equatorward meridional wind anomalies to its northwest and southwest corners. As a result, a poleward bifurcation of two cyclonic circulation anomalies with one in the East Asia and the other near Australia stands out in the following sequence. Notwithstanding, such a poleward pattern later refracts back from the higher latitudes and eventually forms an arc with significant downstream amplification towards North and South Americas (phase 3).

Contrasting to the eastward propagating tendency in the IP Run, the appearance of retrogressive zonal wind anomalies in the equatorial Pacific is also noted. In addition, the convectively-coupled waves seen in both IP and PO Runs are completely absent in the equatorial wave guide regions from the IO Run. The former is caused by the alternation of tropical forcing between eastern Maritime Continent and Amazon basin (signified by the large rainfall anomalies) linked together by the subtropical wave activity described previously. The latter implies that an interactive Pacific Ocean is necessary for providing a feedback mechanism to enhance the convectively coupled waves along the Pacific ITCZ.

References

Flatau, M., P. Flatau, P. Phoebus, and P. Niiler, 1997: The feedback between equatorial convection and local radiative and evaporative processes: The implications for intraseasonal oscillations. *J. Atmos. Sci.*, **54**, 2373–2386.

Hendon, H. H., 2000: Impact of air–sea coupling on the Madden–Julian oscillation in a general circulation model. *J. Atmos. Sci.*, **57**, 3939–3952.

Hsu, H.-H., B. J. Hoskins, and F.-F. Jin, 1990: The 1985/86 intraseasonal oscillation and the role of the extratropics. *J. Atmos. Sci.*, **47**, 823-839.

Inness, P. M., J. M. Slingo, E. Guilyardi, and Jeffrey Cole, 2003: Simulation of the Madden–Julian oscillation in a coupled general circulation model. Part II: The role of the basic state. *J. Climate.*, **16**, 365–382.

Kemball-Cook, S., B. Wang, X. Fu, 2002: Simulation of the ISO in the ECHAM4 model: The impact of coupling with an ocean model. *J. Atmos. Sci.*, 59, 1433-1453.

Madden, R. A., and P. R. Julian, 1994: Observation of the 40–50-day tropical oscillation—A review. *Mon. Wea. Rev.*, **122**, 814–837.

Maloney, E. D., 2002: An intraseasonal oscillation composite life cycle in the NCAR CCM3.6 with modified convection. *J. Climate.*, **15**, 964–982.

Matthews, A. J., and G. N. Kiladis, 1999: The

tropical–extratropical interaction between high frequency transients and the Madden–Julian oscillation. *Mon. Wea. Rev.*, **127**, 661–677.

Rui. H., and B. Wang, 1990: Development characteristics and dynamic structure of tropical intraseasonal convection anomalies. *J. Atmos. Sci.*, 47, 357-379.

Slingo, J. M. and Co-authors, 1996: Intraseasonal oscillations in 15 atmospheric general circulation models: Results from an AMIP diagnostic subproject. *Climate Dyn.*, **12**, 325–357.

Waliser, D. E., K. M. Lau, and J.-H. Kim, 1999: The influence of coupled SSTs on the Madden–Julian oscillation: A model perturbation experiment. *J. Atmos. Sci.*, **56**, 333–358.

Waliser, D. E., K. M. Lau, W. Stern, and C. Jones, 2003: Potential predictability of the Madden–Julian oscillation. *Bull. Amer. Meteor. Soc.*, **84**, 33–50.

Wang, B., and H. Rui, 1990: Synoptic climatology of transient tropical intraseasonal convection anomalies. *Meteor. Atmos. Phys.*, 44(1-4), 43-61.

Wang, B., and X. Xie, 1998: Coupled Modes of the Warm Pool Climate System Part I: The Role of Air-Sea Interaction in Maintaining Madden-Julian Oscillation. *J. Climate*, 11, 2116-2135.

Woolnough, S. J., J. M. Slingo, and B. J. Hoskins, 2000: The relationship between convection and sea surface temperature on intraseasonal timescales. *J. Climate.*, **13**, 2086–2104.

Yu, J.-Y., and C. R. Mechoso, 2001: A coupled atmosphere–ocean GCM study of the ENSO cycle. *J. Climate.*, **14**, 2329–2350.

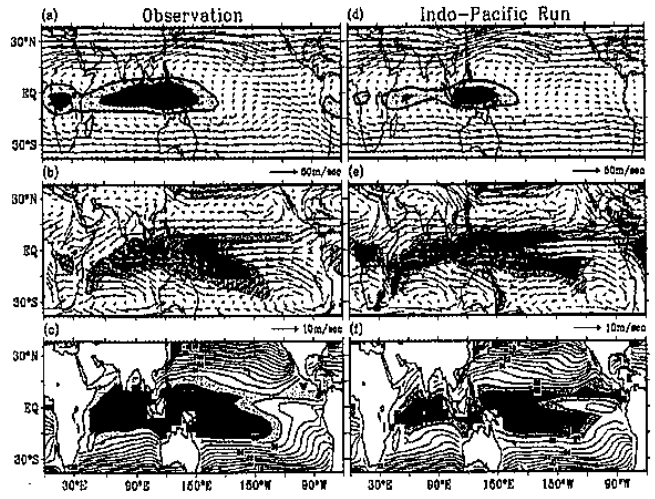

FIG. 1. The observed mean state of (a) 200-mb and (b) 850-mb winds depicted by ERA40 (1979-to-2001), and (c) SST distribution (OISST version 2, 1981-to-2001) during the November-to-April period. Superimposed on (a) is the veritical shear of zonal wind (Us ≡ U200 − U850) shaded with (light, medium, heavy) gray where the Us is smaller than (0, -5, -10) m/sec, and (b) the CMAP rainfall estimates shaded with (light, medium, heavy) gray where rainfall rate exceeds (5, 7.5, 10) mm/day. The corresponding 30-year means from the Indo-Pacific run are shown in the right panels ((d)-to-(f)). Note that the tropical westerlies at 850-mb (in (b) and (e)) are drawned as white vectors.

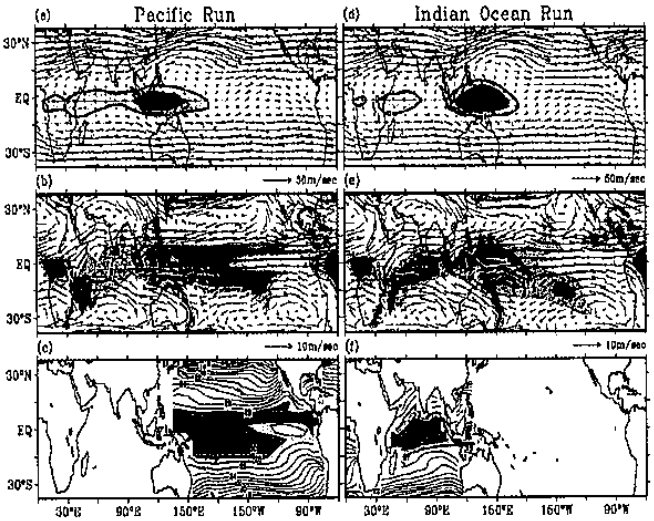

FIG. 2. Configurations are the same as those in FIG.. 1., except for the Pacific run (left panels) and Indian Ocean run (right panels).

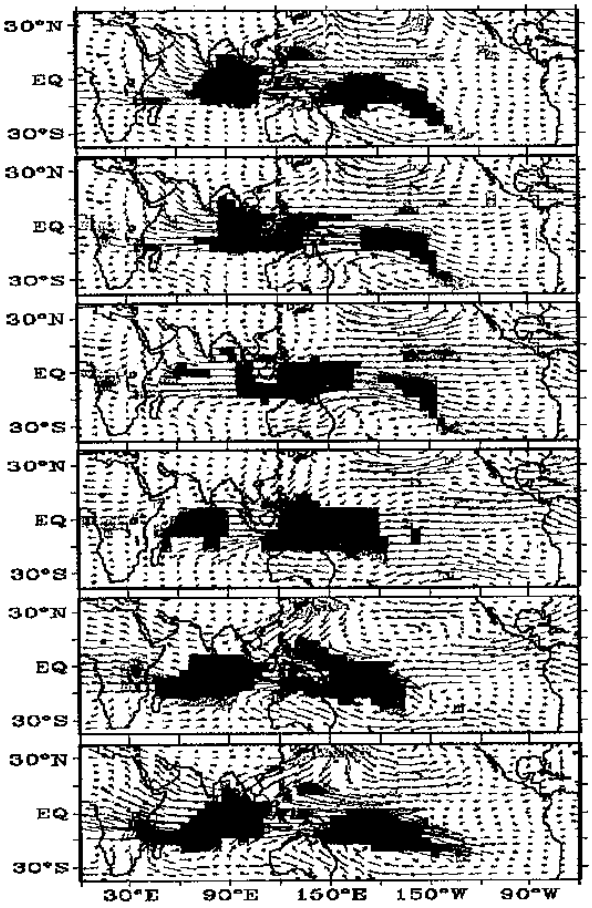

FIG. 3. Composited MJO event of the observed 850-mb wind and rainfall rate anomalies in terms of the first EEOF mode of intraseasonal Us anomalies (30E-to-180, 30S-to-30N) with ± 5 pentad lags in the November-to-April period are shown for the first 6 phases only (downward in order; i.e., from -25-day to 0-day) only).

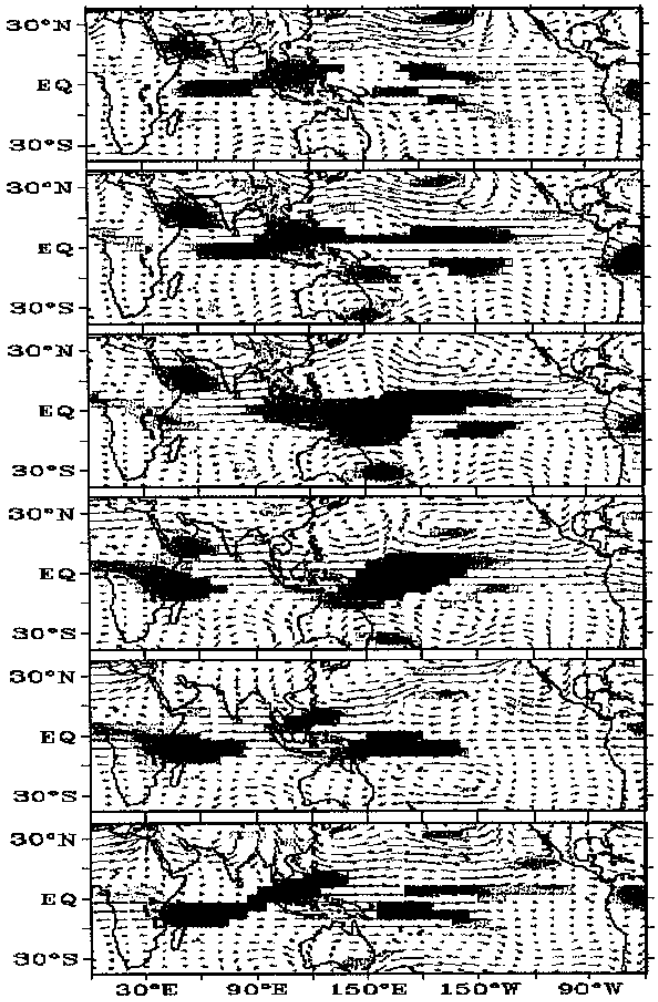

Fig. 4: Same as Fig. 3, except for the Indo-Pacific Run.

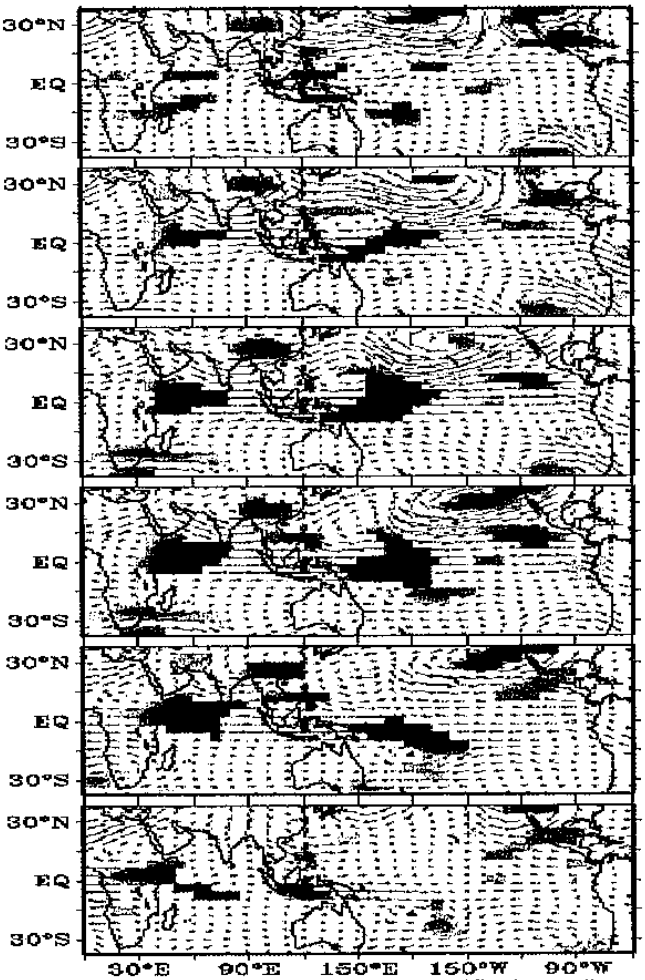

Fig. 5: Same as Fig. 3, except for the Pacific Ocean Run.

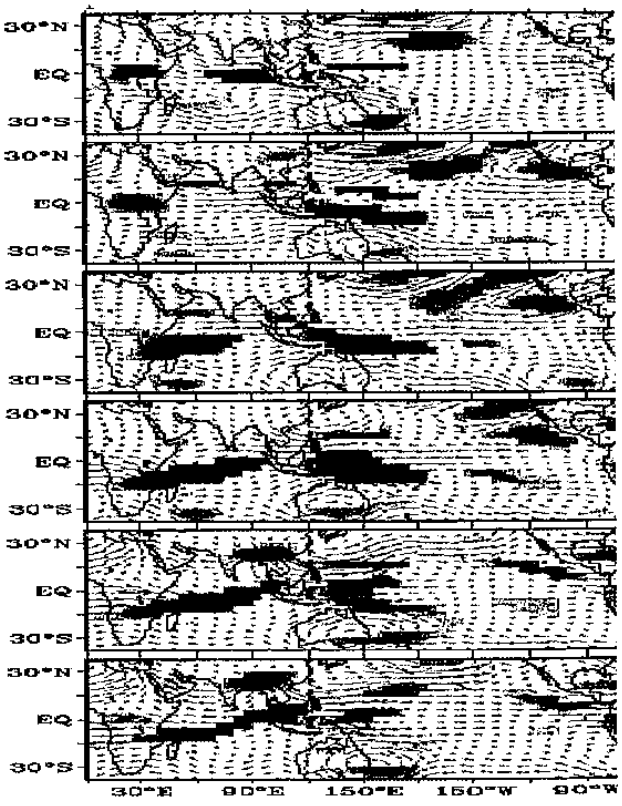

Fig. 6 Same as Fig. 3, except for the Indian Ocean Run.